Angular quasi-phase-matching

Yannick Petit,[1] Benoît Boulanger,[1] Patricia Segonds,[1] and Takunori Taira[2]
[1]*Institut Néel / CNRS-UJF, Boîte Postale 166, F 38042 Grenoble Cedex 9, France*
[2]*Institute for Molecular Science, 38 Nishigonaka, Myodaiji, Okazaki, 444-8585, Japan*
(Received 30 April 2007; published 20 December 2007)

We propose a generalization of quasi-phase-matching of quadratic nonlinear processes that we call angular quasi-phase-matching (AQPM). It corresponds to a propagation of three collinear interacting electromagnetic waves in a periodically poled nonlinear medium at any angle with respect to the grating vector. AQPM directions are analyzed using groups theory.

DOI: 10.1103/PhysRevA.76.063817 PACS number(s): 42.65.Ky, 42.70.Mp, 77.84.Dy

I. INTRODUCTION

Until the 1990's, birefringence-phase-matching (BPM) was the only way to obtain high conversion efficiency in nonlinear media which were single crystals, mainly $LiNbO_3$, KH_2PO_4, $KTiOPO_4$, βBaB_2O_4, and LiB_3O_5 [1]. However, BPM forbids the access to the highest coefficient of the second order electric susceptibility tensor. Such a limitation was overcomed by using quasi-phase-matching (QPM) [2], which was initiated at the beginning of nonlinear optics and developed over the last fifteen years [3]. Nowadays, QPM is mainly realized in $LiNbO_3$ [3], $KTiOPO_4$ [4], and GaAs [5] crystals, where it is possible to periodically reverse the sign of the second order nonlinear coefficients. Efficient devices, based on periodically poled $LiNbO_3$ (PPLN) or periodically poled $KTiOPO_4$ (PPKTP), are now commercially available. Meanwhile advances in the periodic poling process have led to longer and larger PPLN or PPKTP samples, a continuous tuneability of devices using these crystals is difficult to obtain. In previous works, we showed that it is possible to improve the QPM tuneability and beam quality by varying the angle between the grating vector of the periodic poling and the input laser beam axis, the PPLN and PPKTP samples being cut as centimetric cylinders [6,7]. Up to now, the rotation was limited to the plane orthogonal to the domains because the sample depth was too small, of about 500 μm in PPLN and 1 mm in PPKTP. Progress in PPLN design has continued since that time, and today we can prepare PPLN samples with a more important depth of about 5 mm [8]. This good result is an important issue, because it allows us to use pump laser beams with a larger aperture, and so with a higher energy. Moreover it provides a generalization of the QPM concept, which can be realized in deep PPLN samples at any angle with respect to the grating vector. We call this scheme angular quasi-phase-matching (AQPM). The present paper is first devoted to the analysis of AQPM including topology aspects. Then it is applied to second harmonic generation in PPLN in order to illustrate its potentiality.

II. MOMENTUM CONSERVATION

A. Collinear and noncollinear schemes

We are interested in three-wave nonlinear parametric interactions occurring in a nonlinear medium where the sign of the second order electric susceptibility is periodically reversed. In this case, the momentum conservation is given by the following vectorial relation [2]:

$$\vec{k_3} - \vec{k_1} - \vec{k_2} - \vec{k_\Lambda} = \vec{0}, \tag{1}$$

where $\vec{k_\Lambda}$ is the grating vector. $\vec{k_1}$, $\vec{k_2}$, and $\vec{k_3}$ are the wave vectors of the three interacting waves at the wavelengths λ_1, λ_2, and λ_3, respectively, which are linked by the relation $\lambda_1^{-1}+\lambda_2^{-1}=\lambda_3^{-1}$ corresponding to the energy conservation. With also the momentum conservation, the nonlinear process is optimized from the interferences point of view, since the second order nonlinear polarization is in phase with the electric field of the wave radiated by the nonlinear polarization itself.

Generally, QPM is achieved in only one direction of propagation [one-dimensional (1D) access] that is along the grating vector [3,4]. However, we have shown the ability to propagate the three interacting waves in successive directions of the plane containing the grating vector (2D access). It was performed in a PPKTP optical parametric oscillator (OPO) [6] as well as in a PPLN optical parametric generator (OPG) [7] and has led to the broadest continuous spectral tuneability that has been possible up to now. We also experimentally observed that with 2D-access QPM, the signal, idler and pump wave vectors remain collinear, and that even for values of angles of propagation greater than 30° with respect to the grating vector. This is a collinear scheme which was effective in the PPKTP OPO [6], but also in the PPLN OPG where no resonator forced the signal and idler beams to be generated collinearly to the pump one [7]. Our observations were corroborated by the perfect agreement reported between the calculation of the tuning curves using a collinear scheme and the experimental data recorded in both OPO and OPG [6,7]. Obviously, a noncollinear scheme, where $\vec{k_1}+\vec{k_2}$, $\vec{k_3}$, and $\vec{k_\Lambda}$ are not collinear as shown in Fig. 1, was also used for the previous calculations based on the theoretical developments of Ref. [3]. We found the same tuning curve of the 2D-access QPM in PPKTP using the collinear or noncollinear schemes [6]. Then according to the typical wavelength dispersion of the refractive indices of PPKTP, the authorized angles between the three interacting vectors are usually very small, so that the noncollinear scheme is similar to the collinear one, which is also true for PPLN.

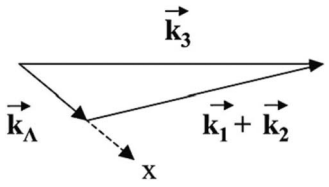

FIG. 1. Noncollinear AQPM; $\vec{k}_\Lambda$ is the grating vector; $\vec{k}_1$, $\vec{k}_2$, and $\vec{k}_3$ are the wave vectors of the three interacting waves.

B. Collinear AQPM

We propose to generalize 2D-access QPM to a 3D-access QPM that we called AQPM, the grating vector being along the x axis as shown in Fig. 2(a). In the case of 2D-access QPM, the directions of propagation are located in the x-y plane of the PPLN or PPKTP crystals only. However, AQPM corresponds to the case where any direction of propagation with respect to the grating can be considered, the wave vectors of the three interacting waves being collinear each to the others as shown in Fig. 2(b). The possibility of a collinear scheme for 2D- or 3D-access QPM at oblique incidence with the grating vector can be easily understandable by successively considering the two first domains of the periodically poled medium. Any optical parametric interaction can be considered, and sum-frequency generation is taken as an example here. The two incident waves at the circular frequencies ω_1 and ω_2, with the wave vectors $\vec{k}_1$ and $\vec{k}_2$ collinear each to the other and perpendicularly to the input surface of the crystal, are both refracted into the first domain in the same direction, without any deviation according to the Snell law. Thus the nonlinear polarization wave, whose wave vector is $\vec{k}_1+\vec{k}_2$, propagates in the same direction. If this direction is not a phase-matching direction, there is a phase mismatch $\vec{\Delta k}$ between the nonlinear polarization and the radiated wave at $\omega_3=\omega_1+\omega_2$, whose wave vector can be expressed as $\vec{k}_3=(\vec{k}_1+\vec{k}_2)+\vec{\Delta k}$. Then by taking into account only the radiated field that is collinear to the nonlinear polarization, the previous vectorial relation reduces to a scalar one, where

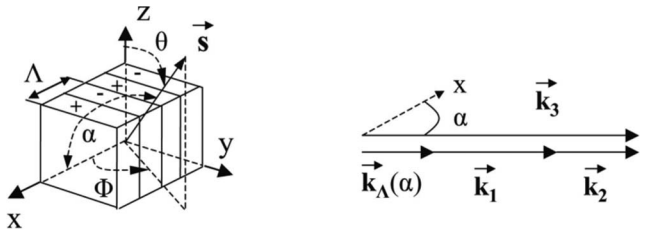

(a) (b)

FIG. 2. Collinear AQPM configuration. (a) Scheme of the periodically poled medium where Λ is the inverting periodicity; $\vec{s}$ is the unit vector of the direction of propagation of the three interacting waves; the angles θ and ϕ are the angles of spherical coordinates in the dielectric frame (x,y,z) of the direction of propagation; α is the angle between the direction of propagation $\vec{s}$ and the x axis. (b) $\vec{k}_\Lambda(\alpha)$ is the effective grating vector in the direction of propagation, and $\vec{k}_1$, $\vec{k}_2$, and $\vec{k}_3$ are the wave vectors of the interacting waves.

$\Delta k(\theta,\phi)=k_3(\theta,\phi)-k_1(\theta,\phi)-k_2(\theta,\phi)$ is the phase mismatch in the direction of propagation with the unit vector $\vec{s}(\theta,\phi)$, where (θ,ϕ) are the angles of spherical coordinates. Actually, since only one domain is considered, these considerations are exactly the same ones used in a homogeneous medium [2]. Furthermore, between the first and second domains, there is no discontinuity of the values of the refractive indices, the periodic poling affecting only the sign of the second order electric susceptibility. As a consequence, the three interacting waves are refracted into the second domain in the same direction than that of the incident ones, and this is true for any value of the angles between $\vec{s}(\theta,\phi)$ and the grating vector. So the three interacting waves are still collinear, and the phase mismatch of the first domain remains the same in the second one. The general idea of QPM is then to use the coherence length, i.e., $l_c=\frac{\pi}{\Delta k}$, of the considered interaction as equal to the length of each domain in order to get phase matching between the nonlinear polarization and the radiated field at each interface between domains [2]. This length has obviously to be taken in the direction of propagation of the waves $\vec{s}(\theta,\phi)$. Thus the periodicity to consider is not Λ, which is along the grating vector $\vec{k}_\Lambda$, but it has to be the effective periodicity $\Lambda(\theta,\phi)=2l_c(\theta,\phi)=\left|\frac{\Lambda}{\sin\theta\cos\phi}\right|$ along $\vec{s}(\theta,\phi)$, corresponding to an effective grating vector $\vec{k}_\Lambda(\theta,\phi)=\frac{2\pi}{\Lambda(\theta,\phi)}\vec{s}(\theta,\phi)$. Then the vectorial relation (1) reduces to the following scalar equation:

$$\frac{n_3(\theta,\phi)}{\lambda_3}-\frac{n_1(\theta,\phi)}{\lambda_1}-\frac{n_2(\theta,\phi)}{\lambda_2}-\frac{1}{\Lambda(\theta,\phi)}=0. \qquad (2)$$

Note that Eq. (2) corresponds to AQPM that is a 3D-access QPM. Thus it is also valid in the two classical QPM cases: 2D access in the xy plane, i.e., $\Lambda(\theta=90°,\phi)=\left|\frac{\Lambda}{\cos\phi}\right|$ [6,7], and 1D access along the x axis, i.e., $\Lambda(\theta=90°,\phi=0°)=\Lambda$ [2,3]. It is valid in BPM, corresponding to $\Lambda\to\infty$.

Equation (2) shows that the angular tunability over θ and ϕ induces a tunability of the refractive indices $n_i(\theta,\phi)$ as well as of the effective periodicity $\Lambda(\theta,\phi)$. This provides two useful degrees of freedom which increase the potentiality of optical parametric interactions as it is shown in the following sections.

III. CONFIGURATIONS OF POLARIZATION AND EFFECTIVE COEFFICIENT

Due to the implication of $\frac{1}{\Lambda(\theta,\phi)}$ in Eq. (2), there are no restrictions, contrary to the case of BPM, dealing with the possible combinations of refractive indices when combining Eq. (2) with $\lambda_1^{-1}+\lambda_2^{-1}=\lambda_3^{-1}$ corresponding to energy conservation. Since for each wave i there are two possible values of the refractive index n_i^+ and n_i^- that are given by the solutions of Fresnel equation [8], then 2^3 combinations are possible: type I $\{n_3^-,n_1^+,n_2^+\}$, type II $\{n_3^-,n_1^-,n_2^+\}$, type III $\{n_3^-,n_1^+,n_2^-\}$, type IV $\{n_3^-,n_1^-,n_2^-\}$, type V $\{n_3^+,n_1^+,n_2^+\}$, type VI $\{n_3^+,n_1^-,n_2^+\}$, type VII $\{n_3^+,n_1^+,n_2^-\}$, and type VIII $\{n_3^+,n_1^-,n_2^-\}$. Of course, in the case of BPM, corresponding to $\Lambda\to\infty$, only three types are possible: Types I, II, and III, corresponding to the usual case of a normal dispersion, i.e., $\frac{\partial n_i}{\partial\lambda}<0$ [9].

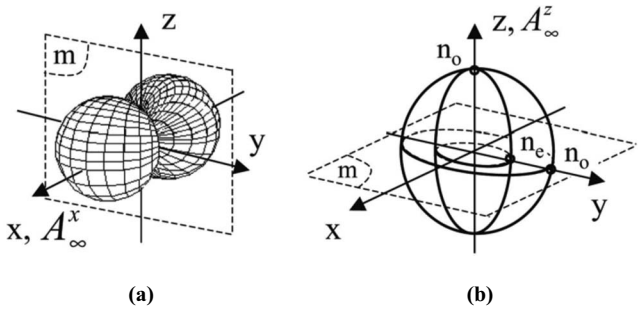

FIG. 3. (a) Angular distribution of $\frac{1}{\Lambda(\theta,\phi)}$ [μm^{-1}]; A^x_∞ is the infinite symmetry axis along the x axis that is the grating vector; m stands for the symmetry mirror orthogonal to the A^x_∞ axis; all the mirrors are not indicated for more legibility. (b) Ordinary and extraordinary layers of the index surface of a negative uniaxial crystal; n_o and n_e are the ordinary and extraordinary principal refractive indices, respectively; all the possible mirrors are not indicated for more legibility.

The eight types of AQPM exhibit different conversion efficiencies due to different angular and spectral acceptances, and also to different effective coefficients. The effective coefficient is defined as

$$\chi_{\text{eff}} = (\vec{e_3} \otimes \vec{e_1} \otimes \vec{e_2}) \cdot \chi^{(2)}. \tag{3}$$

$\vec{e_1}, \vec{e_2}$, and $\vec{e_3}$ are the unit electric field vectors of the three interacting waves and $\chi^{(2)}$ is the second order electric susceptibility tensor, $(\otimes)$ and $(\cdot)$ being tensorial and contracted products, respectively. The acceptances and effective coefficients depending on the direction of propagation, it is then of prime importance to consider any direction of propagation in order to select the most potential one. Note that the configuration of polarization classically used in the case of 1D or 2D access in PPLN or PPKTP is type IV because the corresponding effective coefficient reduces to χ_{33} that is the highest nonlinear coefficient [3,4,6,7]. However, the associated spectral acceptance is not so high, which can reduce the conversion efficiency when the parametric interaction is achieved in the femtosecond regime. Furthermore, it has been shown that using, for example, type I instead of type IV allows the emission bandwidth of QPM SHG in MgO-doped PPLN to be enlarged by a factor of about 4, the involved nonlinear coefficient being χ_{31} [11].

IV. SYMMETRY AND TOPOLOGY ANALYSES

A. Symmetry groups

The symmetry of the space of solutions of the AQPM angles $S_{\text{AQPM}}(\theta,\phi)$ formed by all the AQPM directions, can be determined on the basis of groups theory, by considering the group of orientation symmetry of the four angular functions of Eq. (2). The surface corresponding to the function $\frac{1}{\Lambda(\theta,\phi)}$ belongs to the infinite symmetry group $G_\Lambda = \frac{A^x_\infty}{m} \infty m$, as shown in Fig. 3(a). This is also the group of the cylinder, and it is one of the seven groups of infinite symmetry [12]: A^x_∞ means that the surface remains unchanged by a rotation of any angle around the x axis, which is collinear to the grating vector; m is a symmetry mirror orthogonal to the x axis; and ∞m means that there are an infinity of mirrors containing the x axis. The angular distributions of functions $\frac{n_i(\theta,\phi)}{\lambda_i}$, with $i=1$, 2 and 3, in Eq. (2) are related to the index surface, which is a double-layer surface, at the wavelengths λ_i [9]. We restrict our discussion here to periodically poled uniaxial crystals, then the index surface is made of an ordinary and extraordinary layers: The ordinary layer is a sphere of radius $n_o(\theta,\phi)=n_o$ for any value of θ and ϕ, while the extraordinary layer is a revolution ellipsoid around the z axis, i.e., $n_e^{-2}(\theta,\phi)=\cos\theta^2 n_o^{-2}+\sin\theta^2 n_e^{-2}$ for any value of ϕ, n_o, and n_e being the ordinary and extraordinary principal refractive index, respectively. The ordinary layer belongs to the infinite symmetry group of the sphere $G_o = \frac{A_\infty}{\infty m} \infty m$ [12]: A_∞ is an infinite symmetry axis with any orientation with respect to the dielectric frame, and ∞m means that there is an infinity of mirrors. The extraordinary layer has the cylinder symmetry $G_e = \frac{A^z_\infty}{m} \infty m$, where A^z_∞ is the infinite symmetry axis along the z axis. Note that G_e and G_Λ only differ from the orientation of their infinite symmetry axis. Two cases are distinguished according to the relative values of n_o and n_e which determine the optical sign of a uniaxial crystal: In a crystal with a negative optical sign, which is the case of PPLN, $\{n^+,n^-\} \equiv \{n_o,n_e\}$ as shown in Fig. 3(b), and a positive optical sign corresponds to $\{n^+,n^-\} \equiv \{n_e,n_o\}$.

B. Topology of the AQPM directions

In the same order of idea than Neumann principle and Curie laws [12], the symmetry group G_{AQPM} of the angular quasi-phase-matching space of solutions $S_{\text{AQPM}}(\theta,\phi)$ is given by the intersection between the symmetry groups G_1, G_2, G_3, and G_Λ of the four surfaces $\frac{n_3(\theta,\phi)}{\lambda_3}$, $\frac{n_1(\theta,\phi)}{\lambda_1}$, $\frac{n_2(\theta,\phi)}{\lambda_2}$, and $\frac{1}{\Lambda(\theta,\phi)}$, of Eq. (2). Then G_{AQPM} is written as

$$G_{\text{AQPM}} = G_3 \cap G_1 \cap G_2 \cap G_\Lambda. \tag{4}$$

The intersection between the groups of orientation symmetry is given by the symmetry elements that are common to all the groups. Three different groups are involved: G_Λ on one hand, and G_o or G_e, for G_1, G_2, and G_3, on the other hand, the overall intersection leading to two different groups as shown in the following subsection. When the three interacting waves are ordinary polarized, which corresponds to AQPM types IV in a positive uniaxial crystal and type V in a negative one, then $G_1=G_2=G_3=G_o$. This group having the highest degree of symmetry, it includes all the symmetry elements of G_Λ, and Eq. (2) reduces to G_Λ itself, i.e., $G_{\text{AQPM}}=G_\Lambda=\frac{A^x_\infty}{m}\infty m$. In this case, the resolution of Eq. (2) leads to AQPM directions that form a cone which the revolution axis is the x axis corresponding to the grating vector. It is shown in Figs. 4(a) and 4(b) giving to representations in a 3D space and in a Wülf diagram, respectively. This topoly of the AQPM space of solutions can be also obtained from the direct intersection of the four surfaces representing the four terms in Eq.(2), which reduces to the intersection between the surfaces of Figs. 3(a) and 3(b). As in the case of BPM,

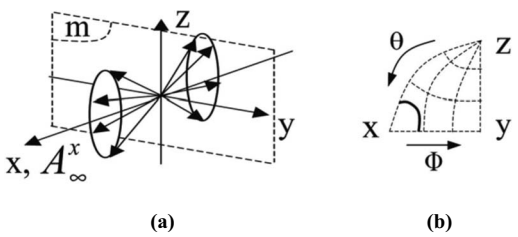

(a) (b)

FIG. 4. Conical distribution of the AQPM directions corresponding to ordinary polarized interacting waves in a periodically poled uniaxial crystal. (a) The 3D representation where the arrows denote some AQPM directions; (x,y,z) is the dielectric frame; A_∞^x is the infinite symmetry axis along the grating vector; m stands for the mirror orthogonal to the x axis. (b) The corresponding representation in a Wülf diagram, where θ and ϕ are the angles of spherical coordinates in the dielectric frame; the continuous line corresponds to the AQPM cone while each dashed lines denotes *loci* with the same value of θ or ϕ.

the existence of loci of AQPM directions depends on the wavelength dispersion of the refractive indices of the considered crystal [10].

For all the other configurations of polarization, that is to say AQPM types I, II, III, IV, VI, VII, and VIII in negative uniaxial crystals, and AQPM types I, II, III, V, VI, VII, and VIII in positive uniaxial crystals, there is at least one extraordinary wave, belonging to G_e. Therefore the intersections of the symmetry groups of Eq. (4) reduce to the three symmetry mirrors that are orthogonal to the principal axes of the dielectric frame. Then $G_{\mathrm{AQPM}}=mmm$, which is a finite symmetry group of the orthorhombic system. The calculation of the corresponding AQPM directions from Eq. (2) leads to three possible topologies. They can be distinguished by their intersections with the principal planes xy, xz, and yz, as shown in Table I: The AQPM directions layer can join xz and xy or yz planes, as well as two directions of the xz plane, according to the polarization states of the interacting waves. The different behaviors of the eight AQPM types are due to specific inequalities between refractive indices that are imposed by Eq. (2). For example, a hypothetical type-VI AQPM direction layer joining the xz and yz planes in a negative uniaxial crystal would impose $\left(\frac{n_1^o}{\lambda_1}+\frac{n_2^o}{\lambda_2}\right)>\frac{n_3^o}{\lambda_3}>\left(\frac{n_1^e}{\lambda_1}+\frac{n_2^o}{\lambda_2}\right)$: It is in contradiction with normal wavelength dispersion law, i.e., $\frac{n_3^o}{\lambda_3}>\left(\frac{n_1^o}{\lambda_1}+\frac{n_2^o}{\lambda_2}\right)$, so that the considered topology is not allowed with type VI for a negative optical sign. Table I also indicates that the symmetry group of the topology corresponding to a junction between xz and xy planes depends on the configuration of polarization: It is $\frac{A_\infty^x}{m}\infty m$ in the case of an $(o\ o\ o)$ configuration, and mmm for all the other configurations of polarization.

The results discussed above illustrate the breaking of symmetry in a uniaxial crystal induced by the grating of the periodical poling well: In the case of BPM, for which there is no grating $(\Lambda\rightarrow\infty)$, the BPM directions form a cone of revolution around the z axis only, whatever the optical sign [10]. In this case, the space of solutions belongs to the same symmetry group than that of the index surface, i.e., $\frac{A_\infty^z}{m}\infty m$, where A_∞^z is an infinite symmetry axis along the z axis. The three possible AQPM topologies shown in Table I, corresponding to the cases where an extraordinary polarized wave at least is involved, also show the breaking of the symmetry of the uniaxial crystal: Actually, the three topologies have the same behaviors than three of the five possible *loci* of BPM in biaxial crystals [9]. This topological similarity is not surprising since the symmetry groups of the space of solutions are the same in the two cases, i.e., the orthorhombic group mmm.

TABLE I. Summary of the possible topologies represented in a Wülf diagram and corresponding symmetry groups of AQPM *loci* according to the type. The two possible optical sign of a periodically poled uniaxial crystal are considered with a grating vector along the x axis and a normal wavelength dispersion; (o) and (e) denote the ordinary and extraordinary polarizations, respectively; (abc), with a, b, and c standing for o or e, is the configuration of polarization corresponding to the wavelengths sequence $(\lambda_3\ \lambda_1\ \lambda_2)$; n_o and n_e are the ordinary and extraordinary principal refractive indices, respectively; $\varnothing$ means that no AQPM directions are allowed.

	I	II	III	IV	V	VI	VII	VIII
$n_e > n_o$	(o e e)	(o o e)	(o e o)	(o o o)	(e e e)	(e o e)	(e e o)	(e o o)
mmm				$\varnothing$				
$\frac{A_\infty^x}{m}\infty m$	$\varnothing$	$\varnothing$	$\varnothing$		$\varnothing$	$\varnothing$	$\varnothing$	$\varnothing$
$n_e < n_o$	(e o o)	(e e o)	(e o e)	(e e e)	(o o o)	(o e o)	(o o e)	(o e e)
mmm					$\varnothing$			
$\frac{A_\infty^x}{m}\infty m$	$\varnothing$	$\varnothing$	$\varnothing$	$\varnothing$		$\varnothing$	$\varnothing$	$\varnothing$

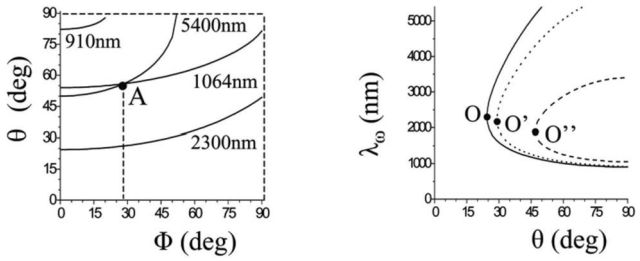

(a) (b)

FIG. 5. Type I SHG AQPM θ and ϕ angles in 7% MgO:PPLN calculated for different fundamental wavelengths λ_ω from the dispersion equation of Ref. [13] using a grating period $\Lambda=15$ μm. (a) θ versus ϕ for four values of λ_ω; dot A corresponds to a direction allowing AQPM for $\lambda_\omega=1064$ nm as well as $\lambda_\omega=5400$ nm. (b) θ versus λ_ω for propagations at $\phi=0°$ (continuous line), $\phi=45°$ (doted line), and $\phi=90°$ (dashed line); dots O, O', and O'' correspond to $\frac{\partial\theta}{\partial\lambda_\omega}=0$.

V. SECOND HARMONIC GENERATION IN PPLN: COMPARISON BETWEEN AQPM AND BPM, 1D- AND 2D-ACCESS QPM

In order to illustrate the potentiality of AQPM, we compared the tunealibility and spectral acceptances of AQPM with BPM and classical QPM in the case of second harmonic generation (SHG) in a periodically poled negative uniaxial crystal: 7% MgO:PPLN with a grating period $\Lambda=15$ μm.

A. Tuneability

The SHG AQPM space of solutions corresponding to the different types were calculated from Eq. (2), by setting $\lambda_1=\lambda_2$ $(\equiv\lambda_\omega)$ and by using the dispersion equations of 7% MgO:PPLN given in Ref. [13]. Note that types-II and III SHG are equivalent since $\lambda_1=\lambda_2$, the situation being the same for types VI and VII. Calculated type-I SHG AQPM curves θ versus ϕ are given in Fig. 5(a) for four values of λ_ω. Figure 5(b) gives type-I SHG AQPM curves λ_ω versus θ for three values of ϕ. We found that type-I SHG AQPM is allowed for fundamental wavelengths ranging between 905 and 5400 nm, the upper wavelength limit being imposed here by the upper limit of the transparency range of the studied material only. The SHG AQPM spectral range was calculated for types II–VIII. It is summarized in Table II.

Table II also gives a comparison between AQPM and BPM in 7% MgO:PPLN by using the same equations of dispersion [13]. Then type I BPM is the only one giving solutions according to the equations of dispersion: we found the possible values of λ_ω ranging between 1050 and 3400 nm. The corresponding tuning curve λ_ω versus θ is the same one than that of AQPM in the $y-z$ plane $(\phi=90°)$ of Fig. 5(b), since the periodicity in that plane is $\Lambda=\infty$ for any value of θ. Note that the effective coefficient, which is given by Eq. (3), is the same for AQPM and BPM: it is reported in Table III for each of the eight types of SHG.

In the case of 1D-access QPM, the wavelength tuneability is achieved by propagating the interacting waves in a single direction of a multigrating or single-fan-shaped-grating crys-

TABLE II. Comparison between BPM and AQPM topologies and spectral range of 7% MgO:PPLN with a grating period of $\Lambda=15$ μm. (o) and (e) denote the ordinary and extraordinary polarizations, respectively. λ_ω and $\lambda_{2\omega}$ are the fundamental and second harmonic wavelengths, respectively. X means that there are no BPM or AQPM solutions using the wavelength dispersion equations of the refractive indices of 7% MgO:PPLN of Ref. [13]. ∅ means that BPM types are not allowed.

Types $(\lambda_{2\omega}\ \lambda_\omega\ \lambda_\omega)$	Phase Matching		Angular Quasi-Phase-Matching	
	λ_ω range	Topology	λ_ω range	Topology
I (e o o)	1050-3400 nm		905 - 1050 nm 1050 - 3400 nm 3400 - 5400 nm	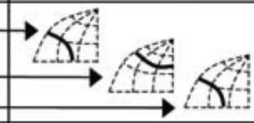
II = III (e e o)	X	X	1075 - 5400 nm	
IV (e e e)	∅	∅	1400 - 5400 nm	
V (o o o)	∅	∅	1510 - 5400 nm	
VI = VII (o e o)	∅	∅	2490 - 4640 nm	
VIII (o e e)	∅	∅	X	X

TABLE III. SHG effective coefficient of PPLN corresponding to all the possible configurations of polarization for AQPM and BPM. Types IV, V, VI, VII, and VIII are not allowed for BPM. The coefficients χ_{ijk} are the independent elements of the second order electric susceptibility tensor of PPLN. ρ_ω and $\rho_{2\omega}$ are the double refraction angles at the fundamental and second harmonic circular frequency, respectively.

Types $(2\omega:\omega,\omega)$	$\chi_{\text{eff}}^{(2)}$
I $(e\ o\ o)$	$\chi_{yyy}\cos(\theta+\rho_{2\omega})\sin\varphi(1-4\cos^2\varphi)+\chi_{zxx}\sin(\theta+\rho_{2\omega})$
II=III $(e\ e\ o)$	$\chi_{yyy}\cos(\theta+\rho_{2\omega})\cos(\theta+\rho_\omega)\cos\varphi(4\sin^2\varphi-1)$
IV $(e\ e\ e)$	$-\chi_{yyy}\cos(\theta+\rho_{2\omega})\cos^2(\theta+\rho_\omega)\sin\varphi(1-4\cos^2\varphi)$ $+(\chi_{xzx}+\chi_{xxz})\cos(\theta+\rho_{2\omega})\sin(\theta+\rho_\omega)\cos(\theta+\rho_\omega)+$ $\chi_{zxx}\sin(\theta+\rho_{2\omega})\cos^2(\theta+\rho_\omega)+\chi_{zzz}\sin(\theta+\rho_{2\omega})\sin^2(\theta+\rho_\omega)$
V $(o\ o\ o)$	$\chi_{yyy}\cos\varphi(1-4\sin^2\varphi)$
VI=VII $(o\ e\ o)$	$\chi_{yyy}\cos(\theta+\rho_\omega)\sin\varphi(1-4\cos^2\varphi)+\chi_{xzx}\sin(\theta+\rho_\omega)$
VIII $(o\ e\ e)$	$\chi_{yyy}\cos(\theta+\rho_1)\cos(\theta+\rho_2)\cos\varphi(4\sin^2\varphi-1)$

tal [14,15]. With a periodicity $\Lambda=15\ \mu$m, the fundamental wavelengths of the different types of 1D-access QPM SHG are the lower limits of the wavelength ranges found for types-I, IV, V AQPM, i.e., 905, 1400, and 1510 nm, respectively, and the two limits of types-VI=VII AQPM: 2490 and 4640 nm, as shown in Table II. Practical tunable 1D-access QPM devices are classically based on type IV. Then periodicities ranging between 4.2 and 30.7 μm must be considered in order to cover the same spectral range than that of AQPM, i.e., from 905 to 5400 nm, using the dispersion equations of Ref. [13]; however, periodicities lower than 15 μm over a depth of few millimetres are not still available.

Since 2D-access QPM, which corresponds to an angular tuneability in the x-y plane, is included in AQPM, their comparison is also directly possible from Table II. 2D-access QPM is possible when the AQPM cone joins the x-y plane with another one. Thus Table II shows that 1050–3400 nm is the only wavelength range for type-I 2D-access QPM to be forbidden in 7% MgO:PPLN. Nevertheless type-II, III, and VIII 2D-access QPM have a nil effective coefficient according to Table III, since $\theta=90°$ and $\rho_{\omega,2\omega}=0°$ in the x-y plane. As a consequence, the associated conversion efficiency is nil for these three types, even if the momentum conservation is achieved. Furthermore, since χ_{zzz} is of about one order of magnitude greater than the other coefficients, it is obvious that type IV is the more interesting one [3,6]. However, type-IV 2D-access QPM is forbidden at fundamental wavelengths located below 1400 nm in 7% MgO:PPLN, while type-I AQPM is allowed until 905 nm.

B. Spectral acceptance

A wide spectral acceptance is necessary to achieve frequency conversion in the femtosecond regime. The behavior

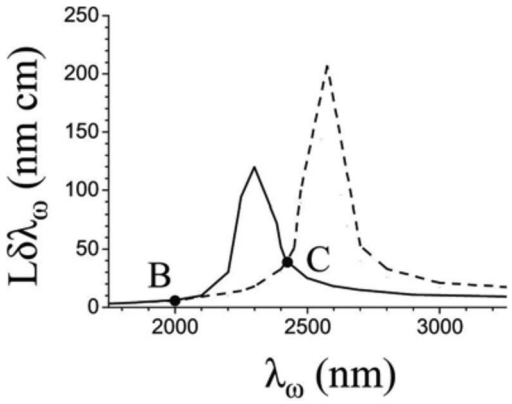

FIG. 6. Spectral acceptance $L\delta\lambda_\omega$ of SHG in 7% MgO:PPLN calculated as a function of the fundamental wavelength λ_ω from the dispersion equation of Ref. [13]. The continuous line curve corresponds to type-I AQPM in the x-z plane of a single-grating crystal with a period $\Lambda=15\ \mu$m rotated from $\theta=24°$ and $\theta=35°$. The dashed line curve refers to type-IV 1D-access QPM along the x axis in a multigrating crystal from $\Lambda=15$ to 30.7 μm, and to a type-IV 2D-access QPM in the x-y plane of a single-grating crystal with a period $\Lambda=15\ \mu$m rotated from $\phi=0°$ and 29°. Dots B and C refer to the intersection between the two curves.

of the AQPM tuning curves θ versus λ_ω of Fig. 5(b) can easily give an idea of the evolution of the spectral acceptance $L\delta\lambda_\omega$ as a function of λ_ω. Indeed, the spectral acceptance, which is defined as the full width $\delta\lambda_\omega$ at 0.405 of the maximum of the curve $\sin c^2(\Delta kL/2)$ versus λ_ω, is directly linked to the derivative of the AQPM tuning curve $\frac{\partial\theta}{\partial\lambda_\omega}$. The three curves of Fig. 5(b), relative to type-I AQPM in the planes at $\phi=0°$ (x-z plane), $\phi=45°$ and $\phi=90°$ (y-z plane), all exhibit a vertical slope, and thus a maximal value of $L\delta\lambda_\omega$, at a given value of λ_ω; these values are, respectively, 2310 nm (dot O), 2230 nm (dot O'), and 1910 nm (dot O''). The corresponding calculated values are 117, 119, and 86 nm cm. The spectral acceptance decreases from either sides of each of these wavelengths, the minimal values being reached at the lower and upper limits of the AQPM spectral range. It is shown in Fig. 6 with the example of a propagation at $\phi=0°$: The fundamental wavelength range corresponds to a rotation of the 7% MgO:PPLN crystal in the x-z plane, from $\theta=90°$ for $\lambda_\omega=905$ nm, to $\theta=24°$ for $\lambda_\omega=2310$ nm, according to the dashed curve of Fig. 5(b). Note that dots O, O', and O'' denote noncritical AQPM situations with respect to wavelength, while it is critical from the angular point of view.

As explained above, the tuning curve of type-I BPM is given by type-I AQPM in the y-z plane ($\phi=90°$). Thus the corresponding spectral acceptances are the same for both of them, i.e., $L\delta\lambda_\omega=86$ nm cm, which is lower than the values of type-I AQPM performed out of the y-z plane.

We calculated the spectral acceptance $L\delta\lambda_\omega$ of 1D-access QPM of type-IV SHG over the possible wavelength range in a multigrating PPLN, with a grating periodicity ranging between 15 and 30.7 μm, in the fundamental wavelength range 1400–5400 nm. The corresponding curve, which is given in Fig. 6, exhibits a maximal value of 207 nm cm at 2575 nm, which corresponds to a grating periodicity $\Lambda=30.7\ \mu$m. This

curve is also that of type-IV 2D access in single-grating PPLN with a periodicity $\Lambda=15$ μm, corresponding to a rotation of the crystal from $(\theta=90°, \phi=0°)$ to $(\theta=90°, \phi=29°)$ using $\Lambda(\theta,\phi)=|\frac{\Lambda}{\cos\phi}|$. This maximum is linked to a vertical slope of the 1D-access QPM curve λ_ω versus Λ, and of the 2D-access QPM curse λ_ω versus ϕ. Figure 6 shows that type-I AQPM exhibits a wider spectral acceptance than type-IV 1D- or 2D-access QPM for fundamental wavelengths ranging between 2000 nm (dot *B*) and 2420 nm (dot *C*). However, type-IV 1D- or 2D-access QPM are better than type-I AQPM for fundamental wavelength bigger than 2420 nm. For this latest range, it is obviously more advantageous to use 1D- or 2D-access QPM. Below 2420 nm, the choice between 1D- or 2D-access QPM and AQPM depends on the request: In term of conversion efficiency, 1D- or 2D-access QPM will be more advantageous than AQPM because the low spectral acceptance will be compensated by the high effective coefficient; however, in terms of the duration of the pulse, it will be better to use type-I AQPM, since the wavelength spreading will be preserved.

VI. CONCLUSION

As a conclusion, we introduced AQPM, which is a generalization of QPM using a single grating. We proposed a topological description of the space of solutions which shows that the AQPM *loci* depend on the symmetries of the index surface and of the grating. This study also shows that by combining QPM and birefringence, AQPM provides additional degrees of freedom to tune optical parametric interactions, leading to spectral ranges and acceptances compared with BPM 1D- and 2D-access QPM. For example, calculations performed in the case of SHG of 7% MgO:PPLN well show that AQPM can significantly enlarge the possible wavelengths range of the parametric processes. In addition to this example, it will be important to perform calculations for other interactions, in particular for optical parametric oscillation. The same approach can also be applied to other periodically poled ferroelectric crystals, such as PPKTP [4], isotropic crystals, such as orientation-patterned GaAs [5] and ZnSe [16], or photonic crystals [17,18].

[1] P. F. Bordui and M. M. Fejer, Annu. Rev. Mater. Sci. **23**, 321 (1993).
[2] J. A. Armstrong *et al.*, Phys. Rev. **127**, 1918 (1962).
[3] M. M. Fejer *et al.*, IEEE J. Quantum Electron. **28**, 2631 (1992).
[4] H. Karlsson and F. Laurell, Appl. Phys. Lett. **71**, 3474 (1997).
[5] L. A. Eyres *et al.*, Appl. Phys. Lett. **79**, 904 (2001).
[6] J. P. Fève *et al.*, Opt. Lett. **26**, 1882 (2001).
[7] J. P. Fève *et al.*, Opt. Lett. **28**, 1028 (2003).
[8] H. Ishizuki, I. Shoji, and T. Taira, Appl. Phys. Lett. **82**, 4062 (2003).
[9] A. Yariv and P. Yeh, *Optical Waves in Crystals* (Wiley, New York, 2002).
[10] J. P. Fève, B. Boulanger, and G. Marnier, Opt. Commun. **99**, 284 (1993).
[11] N. E. Yu *et al.*, Opt. Lett. **27**, 1046 (2002).
[12] A. Authier, *Introduction to the Properties of Tensors, Vol. D of International Tables for Crystallography: Physical Properties of Crystals*, edited by A. Authier (Kluwer Academic, Dordrecht, Netherlands, 2003), Chap. 1.1.
[13] http://www.casix.com/product/prod_cry_linbo3.html
[14] L. E. Myers *et al.*, Opt. Lett. **21**, 591 (1996).
[15] P. E. Powers, T. J. Kulps, and S. E. Bisson, Opt. Lett. **23**, 159 (1998)
[16] A. Mustelier *et al.*, Appl. Phys. Lett. **84**, 4424 (2004).
[17] V. Berger, Phys. Rev. Lett. **81**, 4136 (1998).
[18] R. Lifshitz, A. Arie, and A. Bahabad, Phys. Rev. Lett. **95**, 133901 (2005).